Cancer Research

Pulsed High-Intensity Focused Ultrasound Enhances Delivery of Doxorubicin in a Preclinical Model of Pancreatic Cancer

Tong Li[1], Yak-Nam Wang[1], Tatiana D. Khokhlova[2], Samantha D'Andrea[2], Frank Starr[1], Hong Chen[1], Jeannine S. McCune[3,4], Linda J. Risler[3,4], Afshin Mashadi-Hossein[5], Sunil R. Hingorani[6], Amy Chang[6], and Joo Ha Hwang[2]

Abstract

Pancreatic cancer is characterized by extensive stromal desmoplasia, which decreases blood perfusion and impedes chemotherapy delivery. Breaking the stromal barrier could both increase perfusion and permeabilize the tumor, enhancing chemotherapy penetration. Mechanical disruption of the stroma can be achieved using ultrasound-induced bubble activity—cavitation. Cavitation is also known to result in microstreaming and could have the added benefit of actively enhancing diffusion into the tumors. Here, we report the ability to enhance chemotherapeutic drug doxorubicin penetration using ultrasound-induced cavitation in a genetically engineered mouse model (KPC mouse) of pancreatic ductal adenocarcinoma. To induce localized inertial cavitation in pancreatic tumors, pulsed high-intensity focused ultrasound (pHIFU) was used either during or before doxorubicin administration to elucidate the mechanisms of enhanced drug delivery (active vs. passive drug diffusion). For both types, the pHIFU exposures that were associated with high cavitation activity resulted in disruption of the highly fibrotic stromal matrix and enhanced the normalized doxorubicin concentration by up to 4.5-fold compared with controls. Furthermore, normalized doxorubicin concentration was associated with the cavitation metrics ($P < 0.01$), indicating that high and sustained cavitation results in increased chemotherapy penetration. No significant difference between the outcomes of the two types, that is, doxorubicin infusion during or after pHIFU treatment, was observed, suggesting that passive diffusion into previously permeabilized tissue is the major mechanism for the increase in drug concentration. Together, the data indicate that pHIFU treatment of pancreatic tumors when resulting in high and sustained cavitation can efficiently enhance chemotherapy delivery to pancreatic tumors. *Cancer Res; 75(18); 3738–46. ©2015 AACR.*

Introduction

Pancreatic ductal adenocarcinoma (PDAC) is the fourth leading cause of cancer-related mortality in the United States (1, 2). In 2013, more than 45,000 Americans were diagnosed with pancreatic cancer (2). Unlike many other cancers, the survival rate for PDAC has not improved substantially, with the 5-year relative survival rate for pancreatic cancer increasing from 2% to only 6% since 1975. Although gemcitabine, a deoxycytosine analogue, has been shown to be effective in inducing apoptosis in pancreatic cancer cells *in vitro* and in arresting tumor growth in xenograft (3) and syngeneic mouse models (4–8), its effectiveness in treating pancreatic cancer patients has been disappointing (9, 10). Despite this, it is still the standard chemotherapy used to treat pancreatic cancer.

There are a number of characteristics of pancreatic cancer that make it difficult to treat with chemotherapy; most importantly, is the presence of a dense stroma that separates cancer cells from the blood vessels and significantly decreases tissue permeability (11, 12). The dense stroma has been shown to cause high interstitial pressures that collapse the blood vessels in the tumor, leading to limited blood perfusion and insufficient drug delivery (13). The main reason for the discrepancy in gemcitabine efficiency between human trials and many preclinical animal studies is thought to be due to the absence of a desmoplastic stroma in the xenograft and syngenic autograft models. Recently, a transgenic mouse model of PDAC, that is, KrasLSL.G12D/+; p53R172H/+; PdxCretg/+ (KPC) mouse, was developed that closely recapitulates the genetic mutations, clinical symptoms, and histopathology found in human pancreatic cancer (14). This mouse model is considered one of the most appropriate models for studying drug delivery in pancreatic cancer, because it provides a much more realistic model to evaluate the potential for clinical translation (15). Studies in the KPC mouse model have demonstrated that breaking down the stromal matrix by the administration of smoothened inhibitor, IPI-926, increases delivery of gemcitabine into the tumors (14, 16). It also results in an increase in intratumoral vascular density and intratumoral concentration of gemcitabine 4 days after treatment, leading to stabilization of disease

[1]Center for Industrial and Medical Ultrasound, Applied Physics Laboratory, University of Washington, Seattle, Washington. [2]Division of Gastroenterology, Department of Medicine, University of Washington, Seattle, Washington. [3]Department of Pharmacy, University of Washington, Seattle, Washington. [4]Department of Pharmaceutics, University of Washington, Seattle, Washington. [5]Department of Biostatistics, University of Washington, Seattle, Washington. [6]Fred Hutchinson Cancer Research Center, Seattle, Washington.

Note: Supplementary data for this article are available at Cancer Research Online (http://cancerres.aacrjournals.org/).

Corresponding Author: Joo Ha Hwang, University of Washington, 1959 Northeast Pacific Street, Box 356424, Seattle, WA 98195. Phone: 206-685-2283; Fax: 206-221-3992; E-mail: Jooha@medicine.washington.edu.

doi: 10.1158/0008-5472.CAN-15-0296

and an extended survival from 11 to 25 days. In spite of these promising results, IPI-926 performed poorly in pancreatic cancer clinical trials, resulting in more aggressive tumors, with heightened proliferation, indicating that stromal elements may also restrain tumor growth (17). Thus, the development of efficient strategy for chemotherapeutic drug delivery to pancreatic tumors remains an unmet challenge.

High-intensity focused ultrasound (HIFU) therapy is commonly used as a noninvasive treatment that kills diseased tissue with heat (ablation) or mechanical distruption (cavitation). In HIFU, powerful ultrasound waves from an extracorporeal source are focused transcutaneously to induce thermal or mechanical tissue damage at the focus without affecting surrounding tissues. Most HIFU treatments use the thermal effect resulting from absorption of continuous ultrasound waves by tissue and have been used to ablate various solid tumors, including pancreatic cancer (18). Alternatively, pulsed HIFU (pHIFU) treatments may be used to promote the mechanical effects, primarily acoustic cavitation—formation and ultrasound-driven activity of micron-sized bubbles in tissue. Although live tissue does not initially contain gas bubbles, tiny gas bodies dispersed in cells may serve as cavitation nuclei that grow into bubbles when subjected to sufficiently large rarefactional pressure, that is, a cavitation threshold (19). The violent collapses of the cavitation bubbles, termed inertial cavitation, can disrupt tissue due to the accompanying high shear forces that are generated, and thus increase tissue and/or vascular permeability (20). In recent years, there has been an increasing interest in using pHIFU with and without microbubbles to enhance drug delivery to solid tumors by permeabilizing the tissue through cavitation (21, 22). However, studies on measuring cavitation activity during *in vivo* studies have been scarce (23).

In a recent study by Tinkov and colleagues (24), ultrasound-induced targeted destruction of doxorubicin-loaded microbubbles was used to enhance localized drug delivery in a rat model with subcutaneously grafted pancreatic carcinoma. A 12-fold higher tissue concentration of doxorubicin and a significantly lower tumor growth in the targeted tumor compared with the contralateral control tumor was observed. However, the animal model used in the study is not ideal for evaluating clinical translation due to the absence of the desmoplastic reaction.

Unlike most other studies on cavitation-enhanced drug delivery, the study described in this article was based on nucleating and sustaining cavitation in the tumor tissue itself, without systemic administration of ultrasound contrast agents (UCA). This choice was dictated by the characteristics of pancreatic cancer—poor vascularization and high interstitial pressure, which made it unlikely for the UCAs to be circulating through the tumor in large enough numbers. Moreover, UCAs are confined to vasculature and may not cause sufficient permeabilization of the stromal matrix, the main obstacle to drug delivery. As cavitation is a stochastic phenomenon, the cavitation threshold, as well as the correlation between drug penetration and the cavitation activity metrics is difficult to establish and is still controversial (21, 25, 26). In our previous studies, we developed a methodology for quantification of cavitation activity in pancreatic tumors during pHIFU using passive cavitation detection (PCD; ref. 23). Here, we aimed to correlate the corresponding cavitation metrics with the enhancement of the chemotherapy uptake, specifically doxorubicin, by the tumor in the KPC mouse model.

Another goal of this study was to investigate the mechanism of pHIFU-enhanced drug delivery: Active diffusion of the drug facilitated by acoustic streaming that accompanies bubble activity versus passive diffusion into permeabilized tissue. We thus compared the drug uptake in two different administration sequences that use either of the mechanisms: Doxorubicin infusion during or after pHIFU treatment.

Materials and Methods

pHIFU system

A preclinical focused ultrasound system (VIFU 2000; Alpinion Medical Systems), was used for pHIFU exposures, treatment planning, and cavitation monitoring. The system, shown in Fig. 1A, was used with either of the two alternative HIFU transducers—

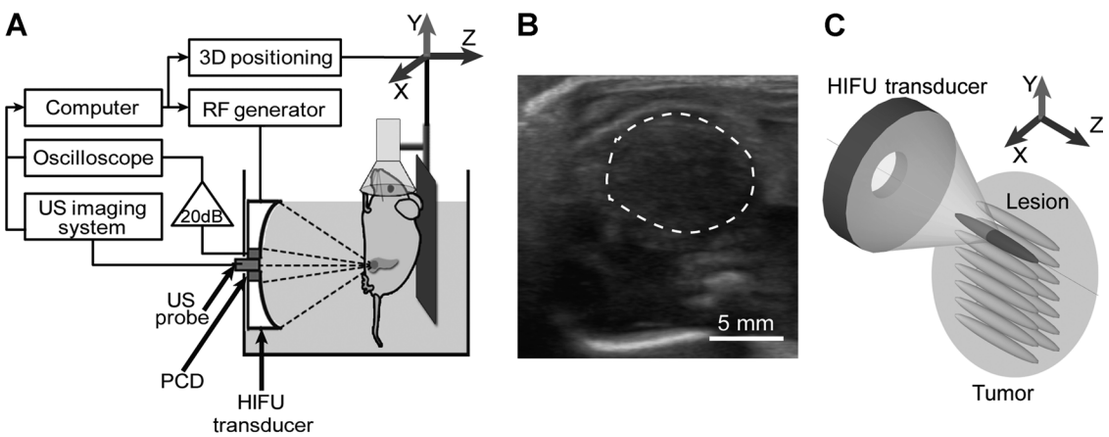

Figure 1.
A, schematic illustration of the pHIFU treatment system. The HIFU transducer, a ring-shaped transducer for PCD, and an ultrasound imaging probe were aligned confocally and coaxially, and built into the side of the acrylic water tank. The anesthetized KPC mouse was placed in a custom holder attached to a 3D positioning system during treatment. B, B-mode ultrasound image of a mouse pancreatic tumor (dashed line). B-mode image guidance was used during treatment to align the targeted tumor region with the HIFU focus. C, the HIFU focal area was scanned in two transverse directions during treatment to cover the tumor region.

a 1.1-MHz transducer (64-mm aperture and radius of curvature) and a 1.5-MHz transducer (64-mm aperture and 45-mm radius of curvature). Both transducers had a circular central opening of 38-mm diameter, which was fitted with a focused ring-shaped transducer for PCD and an ultrasound imaging probe (C4-12 phased array, center frequency: 7-MHz, Alpinion Medical Systems) for in-line targeting of the tumor. The geometric foci of the PCD and the HIFU transducers were aligned in the axial direction, so that the overlap of the focal areas was maximized (23). The transducers were mounted in a water tank attached to a water conditioning system for continuous degassing and heating. HIFU focal pressures were applied between 1.6–12.4 MPa and 2.2–17 MPa for the 1.1- and 1.5-MHz transducers, respectively (27).

Cavitation detection and quantification

The broadband noise emissions associated with inertial cavitation during each pHIFU pulse were received by the PCD transducer, amplified by 20 dB (Panametrics PR5072) as shown in Fig. 1A, recorded by a digital oscilloscope (Picoscope 4424; Pico Technology) and processed as previously reported (23). Briefly, each signal was filtered in the frequency domain to eliminate the signal associated with HIFU waves backscattered from tissue. The filtered PCD signal was further analyzed in time domain to obtain two metrics: A binary evaluation of whether a cavitation event took place within the HIFU pulse and, if a cavitation event was observed, a measure of the cavitation activity in the form of the broadband noise amplitude. The cavitation event was considered observed if the signal amplitude was distinguishable from the maximum amplitude of the background noise by a simple statistical variation of the background noise with a 98% confidence level (28). The measure of cavitation activity was obtained by integration over the broadband noise components in the frequency domain. This metric is similar to that used by Hwang and colleagues (29).

The cavitation metrics obtained for each pulse of a pHIFU treatment were batch-processed to extract the following indicators of cavitation activity at each treated spot: Cavitation persistence and mean broadband noise amplitude. Cavitation persistence was defined as the percentage of the HIFU pulses that induced a cavitation event among the pulses delivered at a single-treatment spot; it was then averaged over all pHIFU focus locations in the tumor.

According to the measurements performed in our previous work, the peak-rarefactional pressure corresponding to the cavitation threshold for the pancreatic tumors in KPC mice (i.e., the probability of inducing a cavitation event at any given spot in the tumor is 50%) at 1.1 MHz was 3 MPa, whereas cavitation persistence reached 50% level at 7 MPa, 75% level at 8.5 MPa and 100% at 11 MPa. Similar preliminary measurements were performed for the 1.5-MHz transducer following the same methodology (23), and the cavitation threshold was found to be 11.5 MPa, with persistence reaching 50% at 13 MPa, 75% at 14.5 MPa and 100% at 16.5 MPa.

Although thorough measurements of cavitation activity were performed previously, there was no estimate of the minimally required cavitation activity to enhance drug penetration into the pancreatic tumor. A preliminary experiment was, therefore, performed, in which the drug was administered during pHIFU exposure of a subcutaneous tumor, and the peak-negative focal pressure varied among treatment spots. The cavitation metrics were recorded at each spot, and the drug penetration was evaluated. On the basis of the results of the preliminary experiment, three acoustic output settings were determined for drug delivery experiments that resulted in low-cavitation dose (cavitation persistence less than 25%), medium-cavitation dose (cavitation persistence of 25%–75%), and high-cavitation dose (cavitation persistence of 75%–100%).

Animal model and experimental design

A KPC transgenic mouse model of PDAC was used. This model closely recapitulates the genetic mutations, clinical symptoms, and histopathology found in human pancreatic cancer, unlike subcutaneous or orthotopic models (14). The tumors have a moderately differentiated ductal morphology with extensive dense stromal matrix and poorly developed vasculature. All of the animal experimental procedures were approved by the Institutional Animal Care and Use Committee at the University of Washington. KPC mice were closely monitored and imaged by high-resolution diagnostic ultrasound to screen for pancreatic tumor development (30); when the tumor size reached 1 cm, the animal was enrolled in the study.

In this study, doxorubicin was used as a chemotherapeutic agent and served as a proxy to gemcitabine because it is conveniently detectable by fluorescent imaging. The molecular weight of gemcitabine is lower than doxorubicin. Therefore, it should be easier for gemcitabine to pass through the vasculature (31, 32). The animals received intravenous infusion of 30 mg/kg doxorubicin via the tail vein either during or after pHIFU treatment. The infusion duration corresponded to that of the pHIFU treatment.

A total of 31 mice were used in this study. All animals were divided into groups ($n = 5$–8) randomly according to the cavitation dose to be delivered during pHIFU treatment—low, medium, or high—and the time of the doxorubicin administration—during or after the pHIFU treatment. The control group received doxorubicin administration only. Mice ($n = 5$) that had large acoustically treatable areas were subject to both types of treatment. In these cases, pHIFU treatment during doxorubicin administration was performed before the pHIFU treatment after doxorubicin administration and each treatment was located in distinctly separate regions of the tumor.

In the preliminary experiment, the lowest acoustic output level and the corresponding cavitation dose, which yields noticeably enhanced penetration of drug into the tumor was determined using a subcutaneous model of pancreatic cancer due to the comparative ease of targeting. Cell lines with epithelial morphology derived from liver metastases (LMP cells) from KPC mice (2×10^6 cells/mL) were injected s.c. in the flank of the WT mouse, and used when tumor sized reached 1 cm (33).

Experimental procedures

The study animal was anesthetized by inhalation of isoflurane, and the abdomen was shaved and depilated. High-resolution ultrasound imaging was performed (L8-17 linear array, center frequency: 12 MHz, Alpinion) to measure the dimensions of the pancreatic tumor and to identify the acoustic window appropriate for the pHIFU treatment (Fig. 1A). Gas-filled bodies are highly reflective to ultrasound, and therefore intestinal loops and the stomach was avoided. To decrease the potential risk of cavitation on the skin in the treatment path, isopropyl alcohol was used to wipe the area before being submerged into the heated water tank (at 37°C) for treatment planning.

Treatment planning was performed under ultrasound image guidance. The HIFU focus was aligned with the center of the tumor in the axial direction. An example of tumor image is outlined in Fig. 1B. The pHIFU treatment grid in the two transverse dimensions was generated to cover the acoustically accessible tumor region (Fig. 1C). Treatment spots were separated by 2 mm.

During the pHIFU treatment, the mouse holder was moved to position the HIFU focus at each of the planned treatment spots. The same pulsing protocol was used at each spot: A series of 60 pulses of 1 ms duration were delivered at a pulse repetition frequency of 1 Hz. The output power was set at the level corresponding to the desired cavitation dose—low, medium, or high. The 1 ms pulse duration and the low duty factor (0.001) were chosen to avoid thermal effects, especially at the larger focal pressure levels, yet retain cavitation. The temperature elevation per pulse and averaged over the 60-second exposure were estimated following the approach in ref. 23 and were 11.9°C and 6°C, correspondingly for the highest output levels (23). The calculation does not account for tissue perfusion, thus, the heating levels are expected to be even lower.

An average surface projection of the tumor area was 1 cm^2, the average pHIFU treatment time was 30 minutes and the average doxorubicin infusion duration was 30 minutes for both treatment types. Immediately after pHIFU treatment and doxorubicin infusion, mice were removed from the water bath. The abdomen of the animal was surgically opened, the vasculature was flushed with saline and the tumor was collected for examination.

Multispectral imaging

The excised tumor was immediately examined with a fluorescent imaging system (Maestro *in vivo* Imaging System; CRi) to obtain the overall distribution of doxorubicin. *Ex vivo* multispectral image cubes were acquired using a dual-filter protocol (445 to 490 nm Ex/515 nm long pass Em; 503 to 555 nm Ex/580 nm long pass Em). The tunable filter was automatically stepped in 10 nm increments and the camera captured images at each wavelength interval with constant exposure. The spectral fluorescence images consisting of the doxorubicin spectra and tumor autofluorescence were unmixed on the basis of their spectral patterns using the provided software and standard protocols (CRi). The resulting distribution of volumetric fluorescent intensity directly showed the distribution of doxorubicin (yellow) in the targeted area versus control area (pink).

However, this measurement was only qualitative. For the quantitative assessment, small (2 mm in diameter) segments of the tumor in the treated and the control area were collected using a biopsy punch, which were analyzed for doxorubicin concentration by high-pressure liquid chromatography mass spectrometry (LC/MS-MS).

Fluorescent microscopy and histologic examination

After multispectral imaging, the samples were immediately embedded in optimum cutting temperature medium and frozen in isopentane cooled on dry ice. Serial sections of 8-μm thickness were taken at various locations throughout the tumor using a Leica CM 1950 Cryostat (Leica Biosystems). At each location, the first section was evaluated by fluorescent microscopy, using a custom filter set (480/40 nm Ex; 605/50 nm Em; dichroic, 505 lp), to visualize the distribution of doxorubicin. The second section was stained with hematoxylin and eosin (H&E) for structural morphology (34). The third section was stained with Masson's trichrome stain for fibrosis evaluation (35). Masson's trichrome stain was used to characterize the potential damage caused by pHIFU to the collagen in the stromal matrix. All slides were visualized with an upright microscope (Nikon Eclipse 80i; Nikon).

Liquid chromatography with tandem mass spectrometry analysis

The doxorubicin concentration in tumor samples was measured using high-pressure LC/MS-MS, as previously described (36) with minor modifications (Supplementary LC/MS-MS analysis).

Because doxorubicin uptake in tumor tissue varied drastically from one mouse to another due to the differences in vasculature density, heterogeneity, and intratumoral pressure, the doxorubicin concentration in the treated area was normalized to the doxorubicin concentration of nontreated area from the same tumor. In this way, the baseline variance across different mice was justified. The association of this normalized uptake with cavitation activity metrics recorded during pHIFU treatments was evaluated.

Statistical analysis

A generalized estimating equation (GEE) was used to estimate the effect of cavitation metrics on doxorubicin uptake (37), as well as the effect of treatment types on the doxorubicin uptake due to the repeated measurement (both treatment types were applied on separate tumor regions on mice with large acoustic windows) on a number of the mice. Two linear models were used: One to evaluate the association between drug uptake and the cavitation metrics and the other to estimate the difference in uptake between the two treatment types. A similar model was developed for cavitation persistence (Supplementary Statistical Analysis for Cavitation Persistence).

The first model was used to compare the efficacy of the two treatment types as measured by the normalized doxorubicin concentration.

$$E[\text{normalized doxorubicin concentration}|CN, Trt] = \alpha_0 + \alpha_1 CN + \alpha_2 Trt \quad (1)$$

Here, CN is the cavitation noise level, and Trt is an indicator variable that equals 1 when pHIFU and doxorubicin treatment were delivered simultaneously and is 0 otherwise. In this model, α_2 is the parameter of interest, which captures the average difference in doxorubicin uptake between the two treatment schemes for a given cavitation noise level.

The second model was used to compare the rate of local uptake of doxorubicin as a function of increase in cavitation noise level between the two treatment types.

$$E[\text{normalized doxorubicin concentration}|CN, Trt] = \beta_0 + \beta_1 CN + \beta_2 Trt + \beta_3 CN \times Trt \quad (2)$$

where β_1 quantifies the association between changes in cavitation noise level and the uptake of doxorubicin for the sequential treatment scheme and $\beta_1 + \beta_3$ characterizes the association between changes in cavitation noise level and doxorubicin uptake for the simultaneous treatment. Therefore, β_3 captures how the association between doxorubicin uptake and cavitation noise level differs between the two treatment types; β_1 and β_3 are the parameter of interest.

The GEE analyses were performed using the statistical package *geepack* in R version 3.1 (38). A *P* value of less than 0.05 was deemed significant. Before this analysis, a single data point with a value beyond the typical range was identified and was excluded from the analysis.

Results

Preliminary experiment

Mice bearing subcutaneous tumors were used for a pilot measurement of the association of doxorubicin uptake on cavitation activity. The doxorubicin distribution was visualized using multispectral imaging and corresponded to the planned treatment pattern (two columns of 9 treatment spots each), shown as blue colored circles with black lines (Supplementary Fig. S1A). The intensity of blue color corresponded to increasing peak-rarefactional pressure levels in the range from 5 to 11 MPa, as shown in the color bar. Cavitation noise level (Supplementary Fig. S1B), as well as cavitation persistence (Supplementary Fig. S1C) increased with the rise in HIFU peak-rarefactional pressure. According to the multispectral image (Supplementary Fig. S1A), doxorubicin uptake, indicated by yellow color, became noticeable when peak-rarefactional pressure became larger than 8 MPa. The fluorescence from doxorubicin was more intense and consistent when peak-rarefactional pressure became larger than 9.5 MPa. These data suggest that noticeable improvement in doxorubicin uptake may be achieved if cavitation persistence exceeds 50%, and more considerable enhancement is associated with cavitation persistence of at least 75%. Thus, in the following experiments, pressure levels just below, equal to or larger than this level were used to cover all the potential cavitation doses (the correlation between treatment levels and cavitation were described in Materials and Methods).

Multispectral imaging

Multispectral imaging demonstrated that the distribution of drug uptake matched well with the targeted treatment area in tumors that had cavitation persistence and noise levels above 75% and 25 mV, respectively. However, there was no difference between areas that were treated with pHIFU during or before doxorubicin administration. Representative photographs and corresponding multispectral images of KPC tumors from control and animals treated at levels resulting in high cavitation persistence and noise levels are shown (Fig. 2). Control tumors (Fig. 2A and B) did not show any evidence of hemorrhage or damage, and the multispectral image did not indicate a significant doxorubicin uptake. Macroscopic evaluation (Fig. 2C) of treated tumors (treated with both types) often revealed hemorrhagic areas corresponding to the treatment region (white dashed line). These areas also showed enhanced fluorescent intensity compared with the nontreated region (Fig. 2D).

Fluorescent microscopy

Examples of fluorescent microscopy images of tumor sections from the control group and the treated group representing the distribution of doxorubicin uptake are shown in Fig. 3. All of the images were compared with sequential sections stained with Masson's trichrome to correlate the drug uptake with structural and histomorphologic changes. Fluorescent evaluation of the control tumor tissues indicated a lack of drug uptake in all tumors (Fig. 3A and B). A representative fluorescent image (Fig. 3A), and

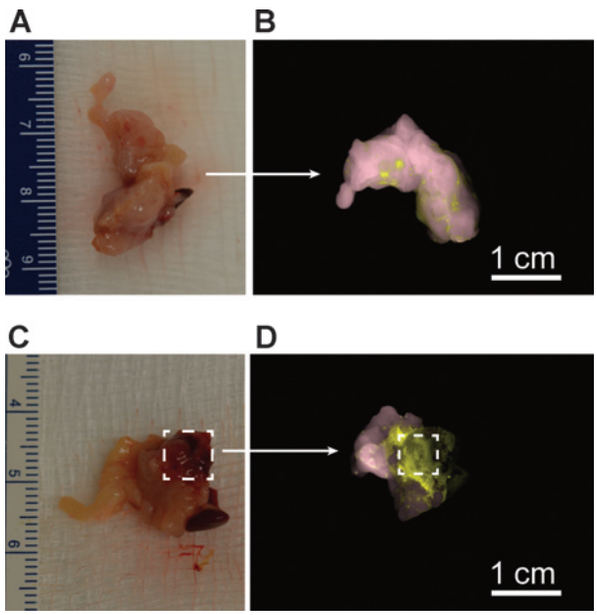

Figure 2.
Photographs and multispectral images of an *in vivo* KPC tumor from the control group (A and B) in which only doxorubicin was administered to the mouse without any pHIFU treatment and treatment group (C and D) in which doxorubicin was administered immediately after pHIFU treatment. The mice were flushed with saline right after euthanasia. In the control example, the photograph (A) and the multispectral image (B) of the tumor showed no significant doxorubicin uptake. The yellow spots that showed some doxorubicin presence corresponded to superficial blood vessels of the tumor that were not successfully flushed (B). In the treatment example, the pHIFU-targeted region (white dashed line) showed significant hemorrhage area in the tumor photograph (C). The fluorescent distribution of doxorubicin (yellow) showed enhanced uptake and corresponds to the targeted area (white dashed line; D).

the corresponding trichrome-stained section (Fig. 3B) are shown. The latter shows an example of a moderately differentiated tumor with the characteristic infiltrative pattern of desmoplastic stroma observed in KPC mice. A higher magnification image is shown in Fig. 3C. Conversely, tumors that had treatments that resulted in high cavitation persistence and noise levels showed evidence of nuclear doxorubicin uptake in treated regions. There was no obvious distinction between the two different treatment types. Figure 3D–F shows representative images from such a treated tumor; a uniform distribution of nuclear doxorubicin uptake is evident (Fig. 3D), and corresponds to an area of disrupted stromal tissue (Fig. 3E). Evaluation at a higher magnification revealed significant damage of the collagen fibers in the form of disorientation and separation of the dense collagen bundles in addition to evidence of fraying of collagen fibers (Fig. 3F). This damage is in contrast with untreated tumors where stromal tissue appears uniform and compact (Fig. 3B). Not only was doxorubicin uptake observed in tumor tissue boundary but also in regions immediately adjacent to areas of large stromal disruption (Fig. 3G–I). Tumors that had treatments resulting in low cavitation persistence and noise levels did not show any evidence of stromal disruption, nor was there evidence of doxorubicin uptake.

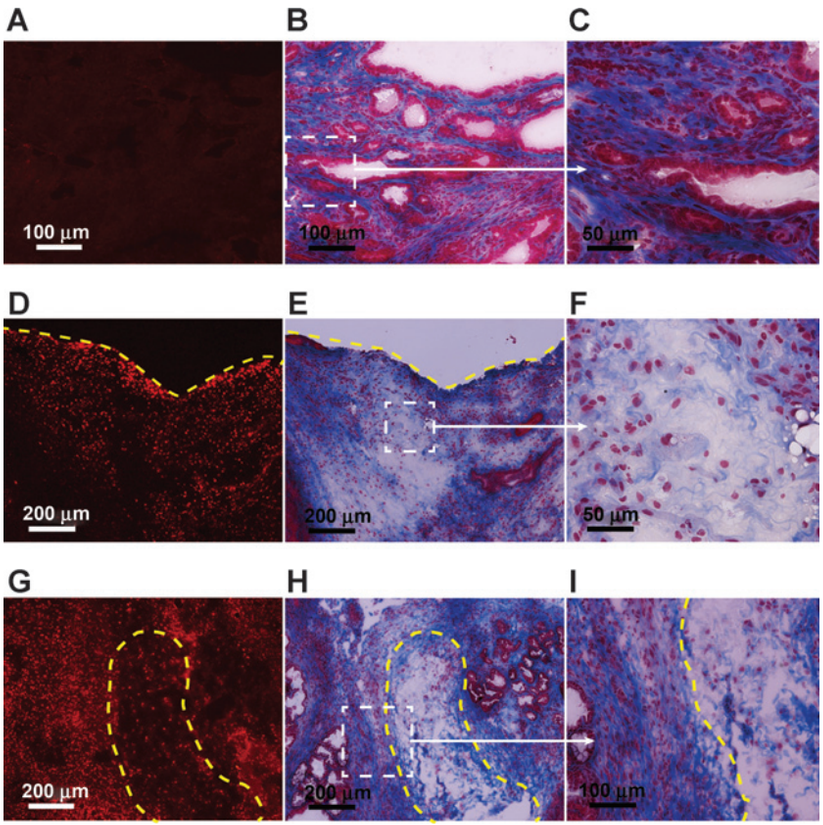

Figure 3.
In the first row, fluorescent image (A) and Masson's trichrome stained image (B) of sequential sections in a nontreated KPC mouse tumor. No significant doxorubicin uptake was observed. The magnification of the Masson's trichrome image (C; higher magnification) showed a dense stromal matrix containing collagen characteristic of pancreatic tumors. In the second row, fluorescent image (D) and Masson's trichrome staining image (E) were taken from sequential sections from a treated KPC mouse tumor. Significant doxorubicin uptake was shown toward the boundary of the tumor (dashed yellow line), but also penetrated into the inner part of the tumor. Masson's trichrome–stained section (E) showed disorientation and separation of the collagen matrix (blue), with fraying of collagen fibrils (F; higher magnification). The nuclear uptake of doxorubicin (D) coincided with this area of stromal disruption. In the third row, representative examples of fluorescent microscopy image (G) and Masson's trichrome–staining image (H) of sequential sections from a treated KPC mouse tumor are shown. A localized area of the tumor disruption by pHIFU was observed (yellow dashed line). The collagen in this area was separated and showed evidence of fraying of the collagen in higher-magnification evaluation (I). Both the area of disruption and the region adjacent to the disrupted area revealed significant nuclear doxorubicin uptake, as shown in G and H.

Doxorubicin uptake into tumors and cavitation metrics

The association of the tumor doxorubicin concentrations, normalized per tumor, with cavitation noise level and cavitation persistence in the control group, and two treatment types groups are shown in scatter plots in Fig. 4A and B, correspondingly. As seen, doxorubicin uptake tends to increase with the increase in both cavitation noise level and cavitation persistence. When the GEE model was applied, the lines corresponding to the GEE solution were plotted, respectively, for the simultaneous treatment and sequential treatment groups (Fig. 4A; Supplementary Fig. S2).

According to the first model, where $\hat{\alpha}_2$ estimates the average (across all cavitation noise level) difference in the uptake of doxorubicin between the two treatment types, the P value of $\hat{\alpha}_2$ was estimated to be 0.52 (Supplementary Table S1), which suggested the difference in the overall drug uptake between the two treatment types were not significant at the 0.05 level.

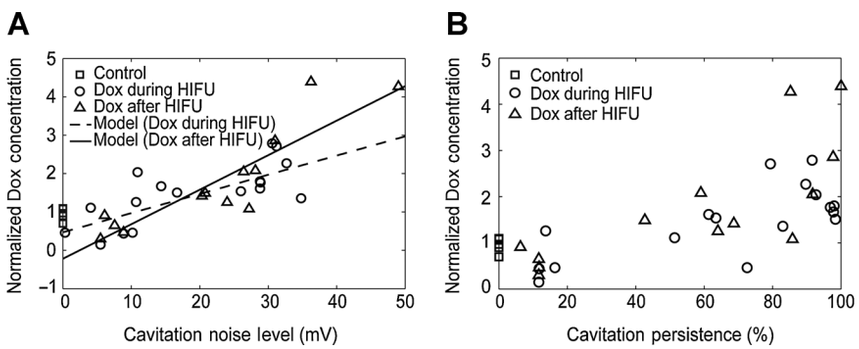

Figure 4.
Scatter plot of normalized doxorubicin (Dox) concentration (the outcome) versus cavitation noise level (A) and cavitation persistence (B). The outcomes tend to increase with both the persistence and the noise level. The data from the control group (squares), outcomes from the simultaneous treatment group (circles), as well as from the sequential treatment group (triangles) are shown. The result lines from the GEE model of cavitation noise level (A) and cavitation persistence (Supplementary Fig. S2) were also plotted for the simultaneous pHIFU treatment and doxorubicin administration (dashed line), and the doxorubicin administration after pHIFU treatment (solid line).

The estimated coefficients from the second model shows $\hat{\beta}_1$ is significant at the 0.05 level ($P < 0.01$), suggesting that cavitation noise level was associated with the doxorubicin uptake (Supplementary Table S2).$\hat{\beta}_1$ being positive is in line with the hypothesis that the more intense the collapse of pHIFU-induced bubbles, the higher the doxorubicin uptake. The value of $\hat{\beta}_3$ suggests that under the simultaneous pHIFU and doxorubicin treatment, the doxorubicin uptake rate per cavitation noise level was in average 0.04 lower than that of the sequential treatment. This estimate was significant at the 0.05 level ($P = 0.01$).

Statistical results were generated for testing the association between cavitation persistence and normalized doxorubicin concentration using a model similar to model 2 (Supplementary Equation S1). This estimate of $\hat{\beta}_1$ is also significant at the 0.05 level ($P < 0.01$), suggesting that cavitation persistence is associated with the doxorubicin uptake, that is, when cavitation bubbles were consistently produced by every pHIFU pulse, drug diffusion was significantly enhanced. The longer the cavitation bubbles persisted, the larger drug uptake it resulted. However, the outcome is not statistically different between two treatment types ($\hat{\beta}_3$; $P = 0.75$).

Discussion

The efficacy and mechanism of pHIFU for enhancing drug delivery to *in vivo* pancreatic tumors were evaluated in a realistic animal model—the KPC mouse model. The results showed that the cavitation metrics (cavitation persistence and cavitation noise level) were associated with an increase in doxorubicin uptake. Multispectral images showed that drug penetration corresponded to the pHIFU-targeted area. Fluorescent microscopy in combination with histologic examination showed that the areas of enhanced doxorubicin uptake were adjacent to and/or in areas where there was evidence of stromal damage. At the highest pHIFU levels, cavitaion noise levels and persistence was found to be consistently above 25 mV and 75%, respectively; at these levels, the drug concentration in the tumor was enhanced 1.5– to 4.5-fold relatively to the untreated areas of the tumor. Hemorrhage was grossly observed in the treated areas, suggesting microvascular rupture inside the tumor. Although intravascular cavitation is known to have the potential of causing capillary rupture, there was no evidence of significant acute bleeding in this study (39). Future studies should analyze the benefits and risks of microvascular rupture in the tumor as it relates to safety and drug delivery.

The results from the two administration sequences (pHIFU treatment followed by drug administration and pHIFU treatment during drug administration) were not statistically different. Two recent publications reported that dense stromal matrix in the tumor applies stress and compresses tumor vessels, and thus restricts perfusion, preventing chemotherapeutic drugs from circulating, and therefore reaching malignant cells (13, 40). We speculate that, in our study, pHIFU-induced cavitation reduced the stress surrounding the tumor vessels by disrupting the stromal matrix, resulting in an increase in tissue perfusion and drug delivery to previously hypoxic areas. With sequential administration of pHIFU followed by doxorubicin, once pHIFU-induced cavitation disrupted the highly fibrotic stromal matrix, tumor perfusion, and permeability could increase, facilitating circulation of the doxorubicin and passive diffusion into the tumor upon drug infusion. With concurrent administration of pHIFU with doxorubicin, when pHIFU treatment was delivered at the same time as doxorubicin infusion, the cavitation-induced streaming, that is, the rapid movement of fluid around the cavitation bubbles could actively enhance drug diffusion from vasculature to stromal tissue, in addition to passive diffusion through gradually permeabilized stromal matrix. The results from both administration sequences demonstrated that the active diffusion by streaming did not result in additional uptake. Therefore, passive drug diffusion through permeabilized tissue was likely the dominant effect for drug delivery. This result has important implications for the clinical implementation of the method in that the tumor can be pretreated with pHIFU, and the drug administration may be performed later without the loss of efficiency. This approach is much simpler and much more feasible logistically compared with the simultaneous administration of pHIFU treatment and drug infusion.

In this work, the combination of multispectral imaging, fluorescent microscopy and LC/MS-MS analysis provided a complementary perspective on the drug delivery by pHIFU in pancreatic tumors. The multispectral imaging detected an integrated fluorescent intensity from doxorubicin over the entire volume of the tumor tissue. The method was used to image overall doxorubicin distribution immediately after the mouse was sacrificed and to confirm whether the distribution corresponded to the targeted region. In all treated tumors with high cavitation noise and persistence levels, enhanced fluorescent intensity corresponding to doxorubicin fluorescence was observed in the treated region as expected. The fluorescent microscopy allowed evaluating the distribution of doxorubicin in the tumor body. Histologic analysis by Masson's trichrome stain showed that the stromal matrix consisting of collagen was disrupted by pHIFU treatment. The doxorubicin uptake observed in the fluorescent imaging was either immediately adjacent or directly corresponded to at the areas of disrupted structure, suggesting that doxorubicin perfused through stromal matrix and penetrated further into the tumor tissue. The results showed that at high cavitation persistence and noise levels resulted in stromal disruption and drug was successfully delivered to cells within the tumor. LC/MS-MS allowed the quantification of doxorubicin concentration in the tumor and showed that pHIFU resulting in high cavitation persistence and high noise level produced the highest doxorubicin uptake by the tumor cells. The spatial distribution of cavitation is likely to be heterogeneous due to the stochastic processes involved and the heterogeneity of the tumor. However, the widespread stromal disruption and doxorubicin uptake observed would suggest that the treatments applied, specifically those with high cavitation persistence and high noise level, allowed sufficient doxorubicin extravasation and penetration to cover the entire treatment region. In addition, it is possible that the spatial distribution of cavitation occurrence can be monitored in real time using a number of new techniques (41, 39), allowing for treatment feedback to help insure that enough stromal tissue is disrupted to enable sufficient diffusion and penetration of the drug.

This study shows that pHIFU can be effective at enhancing the penetration of doxorubicin to pancreatic tumors by stromal disruption. However, further studies must be carried out to evaluate the effectiveness of the treatment in survival studies. It was recently reported that by reducing stromal desmoplasia, tumors exhibited undifferentiated histology but increased vascularity, which may lead to more aggressive tumor growth. However, this could be potentially restrained by antiangiogenesis treatment (17).

Conclusion

In this work, we demonstrated that pHIFU-induced cavitation enhances the concentration of the chemotherapeutic drug doxorubicin in KPC mouse pancreatic tumors by up to 4.5-fold by disrupting the stromal matrix. Normalized doxorubicin concentration was associated with the cavitation metrics and was the largest when pHIFU-induced cavitation persistence reached 100%, that is, cavitation occurred at every delivered HIFU pulse, irrespective of focus location in the tumor, and the broadband noise level during each pulse was large. The study also demonstrated that passive drug diffusion through previously permeabilized tumor tissue is the main mechanism of drug delivery.

Disclosure of Potential Conflicts of Interest

No potential conflicts of interest were disclosed.

Authors' Contributions

Conception and design: H. Chen, J.S. McCune, S.R. Hingorani, J.H. Hwang
Development of methodology: T. Li, Y.-N. Wang, T.D. Khokhlova, F. Starr, H. Chen, J.S. McCune, L.J. Risler, J.H. Hwang
Acquisition of data (provided animals, acquired and managed patients, provided facilities, etc.): T. Li, Y.-N. Wang, T.D. Khokhlova, S. D'Andrea, F. Starr, H. Chen, S.R. Hingorani, J.H. Hwang
Analysis and interpretation of data (e.g., statistical analysis, biostatistics, computational analysis): T. Li, Y.-N. Wang, T.D. Khokhlova, J.S. McCune, A. Mashadi-Hossein, J.H. Hwang
Writing, review, and/or revision of the manuscript: T. Li, Y.-N. Wang, T.D. Khokhlova, H. Chen, J.S. McCune, J.H. Hwang
Administrative, technical, or material support (i.e., reporting or organizing data, constructing databases): Y.-N. Wang, S. D'Andrea, L.J. Risler, A. Chang
Study supervision: J.H. Hwang

Grant Support

This work was supported by the NIH grants 1R01CA154451 and 1K01EB015745 and Washington State Life Sciences Discovery Fund.

The costs of publication of this article were defrayed in part by the payment of page charges. This article must therefore be hereby marked *advertisement* in accordance with 18 U.S.C. Section 1734 solely to indicate this fact.

Received February 1, 2015; revised May 27, 2015; accepted June 30, 2015; published OnlineFirst July 27, 2015.

References

1. Vincent A, Herman J, Schulick R, Hruban RH, Goggins M. Pancreatic cancer. Lancet 2011;378:607–20.
2. Society AC. Cancer facts and figures 2013. Cancer Facts Fig 2013. Society, American Cancer; 2013.
3. Jimeno A, Feldmann G, Suárez-Gauthier A, Rasheed Z, Solomon A, Zou G-M, et al. A direct pancreatic cancer xenograft model as a platform for cancer stem cell therapeutic development. Mol Cancer Ther 2009;8:310–4.
4. Burris HA, Moore MJ, Andersen J, Green MR, Rothenberg ML, Modiano MR, et al. Improvements in survival and clinical benefit with gemcitabine as first-line therapy for patients with advanced pancreas cancer: a randomized trial. J Clin Oncol 1997;15:2403–13.
5. Matano E, Tagliaferri P, Libroia A, Damiano V, Fabbrocini A, De Lorenzo S, et al. Gemcitabine combined with continuous infusion 5-fluorouracil in advanced and symptomatic pancreatic cancer: a clinical benefit-oriented phase II study. Br J Cancer 2000;82:1772–5.
6. Hertel LW, Boder GB, Kroin JS, Rinzel SM, Poore GA, Todd GC, et al. Evaluation of the antitumor activity of Gemcitabine (2′2′-difluoro-2′-deoxycytidine). Cancer Res 1990;50:4417–22.
7. Merriman RL, Hertel LW, Schultz RM, Houghton PJ, Houghton JA, Rutherford PG, et al. Comparison of the antitumor activity of gemcitabine and ara-C in a panel of human breast, colon, lung and pancreatic xenograft models. Invest New Drugs 1996;14:243–7.
8. Suzuki E, Sun J, Kapoor V, Jassar AS, Albelda SM. Gemcitabine has significant immunomodulatory activity in murine tumor models independent of its cytotoxic effects. Cancer Biol Ther 2007;6:880–5.
9. Oberstein PE, Olive KP. Pancreatic cancer: why is it so hard to treat? Therap Adv Gastroenterol 2013;6:321–37.
10. Hidalgo M. Pancreatic cancer. N Engl J Med 2010;362:1605–17.
11. Jacobetz MA, Chan DS, Neesse A, Bapiro TE, Cook N, Frese KK, et al. Hyaluronan impairs vascular function and drug delivery in a mouse model of pancreatic cancer. Gut 2012;62:112–20.
12. Erkan M, Hausmann S, Michalski CW, Fingerle A, Dobritz M, Kleeff J, et al. The role of stroma in pancreatic cancer: diagnostic and therapeutic implications. Nat Rev Gastroenterol Hepatol 2012;9:454–67.
13. Jain RK. An indirect way to tame cancer. Sci Am 2014;310:46–53.
14. Olive K, Jacobetz M, Davidson C. Inhibition of Hedgehog signaling enhances delivery of chemotherapy in a mouse model of pancreatic cancer. Science 2009;324:1457–61.
15. Olive KP, Tuveson DA. The use of targeted mouse models for preclinical testing of novel cancer therapeutics. Clin Cancer Res 2006;12:5277–87.
16. Feldmann G, Dhara S, Fendrich V, Bedja D, Beaty R, Mullendore M, et al. Blockade of hedgehog signaling inhibits pancreatic cancer invasion and metastases: a new paradigm for combination therapy in solid cancers. Cancer Res 2007;67:2187–96.
17. Rhim AD, Oberstein PE, Thomas DH, Mirek ET, Palermo CF, Sastra SA, et al. Stromal elements act to restrain, rather than support, pancreatic ductal adenocarcinoma. Cancer Cell. Elsevier Inc 2014;25:735–47.
18. Khokhlova TD, Hwang JH. HIFU for palliative treatment of pancreatic cancer. J Gastrointest Oncol 2011;2:175–84.
19. Coussios CC, Roy RA. Applications of acoustics and cavitation to noninvasive therapy and drug delivery. Annu Rev Fluid Mech 2008;40:395–420.
20. Pitt WG, Husseini GA, Staples BJ. Ultrasonic drug delivery—a general review. Nature 2004;1:37–56.
21. Khaibullina A, Jang B-S, Sun H, Le N, Yu S, Frenkel V, et al. Pulsed high-intensity focused ultrasound enhances uptake of radiolabeled monoclonal antibody to human epidermoid tumor in nude mice. J Nucl Med 2008; 49:295–302.
22. O'Neill BE, Vo H, Angstadt M, Li KPC, Quinn T, Frenkel V. Pulsed high intensity focused ultrasound mediated nanoparticle delivery: mechanisms and efficacy in murine muscle. Ultrasound Med Biol 2009;35:416–24.
23. Li T, Chen H, Khokhlova T, Wang Y-N, Kreider W, He X, et al. Passive cavitation detection during pulsed HIFU exposures of *ex vivo* tissues and *in vivo* mouse pancreatic tumors. Ultrasound Med Biol 2014;40:1523–34.
24. Tinkov S, Coester C, Serba S, Geis NA, Katus HA, Winter G, et al. New doxorubicin-loaded phospholipid microbubbles for targeted tumor therapy: *in vivo* characterization. J Control Release 2010;148:368–72.
25. Hynynen K. Ultrasound for drug and gene delivery to the brain. Adv Drug Deliv Rev 2008;60:1209–17.
26. Yuh EL, Shulman SG, Mehta SA, Xie J, Chen L, Frenkel V, et al. Delivery of systemic chemotherapeutic agent to tumors by using focused ultrasound: study in a murine model. Radiology 2005;234:431–7.
27. Bessonova O V, Khokhlova VA, Canney MS, Bailey MR, Crum LA. A derating method for therapeutic applications of high intensity focused ultrasound. Acoust Phys 2010;56:354–63.
28. Rose A. Human and electronic vision. New York: Plenum Press; 1974.
29. Hwang JH, Tu J, Brayman AA, Matula TJ, Crum LA. Correlation between inertial cavitation dose and endothelial cell damage *in vivo*. Ultrasound Med Biol 2006;32:1611–9.
30. Sastra SA, Olive KP. Quantification of murine pancreatic tumors by high resolution ultrasound. In:Su GH, editor. Methods Mol Biol. Totowa, NJ: Humana Press; 2013. p. 1–13.
31. Doxorubicin [Internet]. Natl. Cent. Biotechnol. Information.PubChem Compd. Database;CID=31703. [cited 2015 Apr 23]. Available from: http://pubchem.ncbi.nlm.nih.gov/compound/31703#section=Top

32. gemcitabine | C9H11F2N3O4 - PubChem [Internet]. [cited 2015 Apr 23]. Available from: http://pubchem.ncbi.nlm.nih.gov/compound/60750#section=Top
33. Tseng WW, Winer D, Kenkel JA, Choi O, Shain AH, Pollack JR, et al. Development of an orthotopic model of invasive pancreatic cancer in an immunocompetent murine host. Clin Cancer Res 2010;16:3684–95.
34. Fischer AH, Jacobson KA, Rose J, Zeller R. Hematoxylin and eosin staining of tissue and cell sections. CSH Protoc 2008;2008:pdb.prot4986.
35. Vonlaufen A, Joshi S, Qu C, Phillips PA, Xu Z, Parker NR, et al. Pancreatic stellate cells: partners in crime with pancreatic cancer cells. Cancer Res 2008;68:2085–93.
36. Arnold RD, Slack JE, Straubinger RM. Quantification of doxorubicin and metabolites in rat plasma and small volume tissue samples by liquid chromatography/electrospray tandem mass spectroscopy. J Chromatogr B Anal Technol Biomed Life Sci 2004;808:141–52.
37. Hanley JA. Statistical analysis of correlated data using generalized wstimating equations: an orientation. Am J Epidemiol 2003;157:364–75.
38. R Project for Statistical Computing. 2008.
39. Gyöngy M, Coussios C-C. Passive cavitation mapping for localization and tracking of bubble dynamics. J Acoust Soc Am 2010;128:EL175–L180.
40. Chauhan VP, Jain RK. Strategies for advancing cancer nanomedicine. Nat Mater 2013;12:958–62.
41. Li T, Khokhlova TD, Sapozhnikov OA, O'Donnell M, Hwang JH. A new active cavitation mapping technique for pulsed hifu applications—bubble Doppler. IEEE Trans Ultrason Ferroelectr Freq Control 2014;61:1698–708.